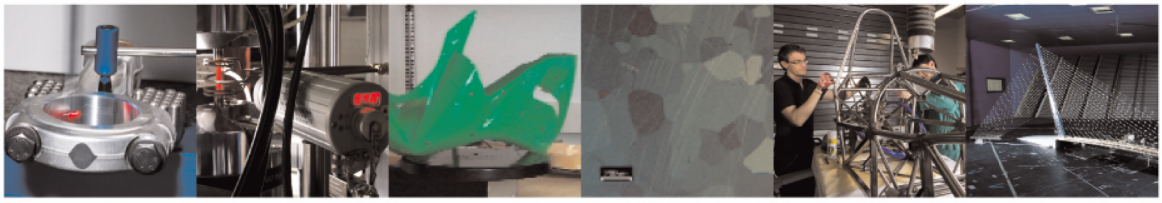

Fatigue Crack Growth Monitoring in Composite Bonded Lap Joints by a Distributed Fibre Optic Sensing System and Comparison with Ultrasonic Testing

A. Bernasconi, M. Carboni, L. Comolli, R. Galeazzi, A. Gianneo and M. Kharshiduzzaman

This is a post-peer-review, pre-copyedit version of an article published in The Journal of Adhesion. The final authenticated version is available online at: http://dx.doi.org/10.1080/00218464.2015.1123153

DIPARTIMENTO DI MECCANICA ■ POLITECNICO DI MILANO
via G. La Masa, 1 ■ 20156 Milano ■ EMAIL (PEC): pecmecc@cert.polimi.it
http://www.mecc.polimi.it
Rev. 0

Fatigue Crack Growth Monitoring in Composite Bonded Lap Joints by a Distributed Fibre Optic Sensing System and Comparison with Ultrasonic Testing

A. Bernasconi, M. Carboni, L. Comolli, R. Galeazzi, A. Gianneo, and M. Kharshiduzzaman
Department of Mechanical Engineering, Politecnico di Milano, Milano, Italy

In this paper, the back-face technique is exploited to monitor fati-gue crack growth (FCG) in a composite, single lap adhesive bonded joint, using distributed sensing by Optical Backscatter Reflectome-try (OBR). Some preliminary results are presented, indicating that, by measuring accurately the strain profile in the overlap region, the correlation between the minimum peak of the strain profile and the position of the crack tip can be exploited for monitoring the struc-tural health of joints. The proposed structural health monitoring technique was validated on the basis of the results obtained by a non-destructive technique using phased array ultrasonic testing (PAUT). The comparison between the two methods yielded encoura-ging results, suggesting that, thanks to its distributed sensing cap-abilities, the OBR technology could allow for improving the back face (BF) technique, as well as any other strain field-based mea-surement technique, for the health monitoring of adhesive joints.

Keywords: Composites, Distributed sensing, Fatigue, Optical backscatter, Ultrasonics

Received 5 August 2015; in final form 18 November 2015.

Address correspondence to A. Bernasconi, Department of Mechanical Engineering, Politecnico di Milano, Via La Masa 1, 20156 Milano, Italy. E-mail: andrea.bernasconi@polimi.it

Color versions of one or more of the figures in this article can be found online at www.tandfonline.com/gadh.

1. INTRODUCTION

Adhesive bonding is one of the most suitable joining techniques for composite lightweight structures. Compared to mechanical joints, it allows for lower stress concentration in the substrates and reduces the dimensions and the weight of connections. However, proper non-destructive testing (NDT) and structural health monitoring (SHM) techniques are required to assess the state of joints, particularly in the case of fatigue loading, when cracks might initiate in the adhesive or in the bonded laminate. The available NDT and SHM techniques, reported in the literature [1] for bonded joints, comprise visual testing (VT), ultrasonic testing (UT), acoustic emission, ultrasonic-guided waves, and strain measurements.

The present research concentrates on the exploitation of the back face (BF) strain technique, as an SHM for bonded joints, and compares its performance with VT and UT [2] as traditional NDT approaches. By the BF strain method [3,4], strain sensors are placed on the BF of adhesively bonded single lap (SL) joints and one possible solution is the adoption of arrays of sensors. Bernasconi et al. [5] monitored fatigue crack growth (FCG) using an array of Fibre Bragg Grating (FBG) sensors on one side of composite adhesively bonded joints. Afterwards, they opted for the BF strain technique to monitor fatigue crack propagation, again by applying an array of FBG sensors, on a Carbon Fibre Reinforced Polymer (CFRP) bonded joint [6]. Similar experiments were performed by Canal et al. [7], by embedding FBG arrays at three different positions through the thickness of the joints. Sans et al. [8] embedded long FBG sensors inside the layer above the crack surface and Stutz et al. [9] applied this technique using an array of FBG sensors to monitor mode I propagation in unidirectional carbon fibre/epoxy Double Cantilever Beam (DCB) specimens. Da Silva et al. [10] measured the strain distribution in adhesive joints using FBG optical sensors.

Instead of using an array of FBG sensors, Chirped Fibre Bragg Grating (CFBG) sensors can be used. Sanderson et al. [11] used CFBG sensors to monitor delamination in unidirectional reinforced glass fibre/epoxy resin DCB specimen. Capell et al. [12] used 60 mm CFBG sensors embedded within glass fibre reinforced plastic (GFRP) adherends to monitor FCG in GFRP/aluminium alloy SL joint and Palaniappan et al. [13] used CFBG sensors to monitor the health of GFRP SL joints.

Another alternative to FBG and CFBG sensors is the Optical Backscatter Reflectometry (OBR) technique, see Güemes et al. [14], which allows for the true distributed sensing of strain along an optical fibre. SHM techniques based on the use of distributed sensing using OBR were presented by Frövel et al. [15] and by Grave et al. [16]. In [17], the BF strain in a woven CFRP SL joint was measured by OBR using a single optical fibre as a sensing unit. The specimen had been subjected to different levels of static loading. Experimental results showed that

the adopted solution has high spatial accuracy in detecting the minimum peak of the BF strain profile. Good agreement between experimental measurements and finite element (FE) analyses was reported, with additional comparison of FE results with Digital Image Correlation strain measurements.

The differences between FBG and OBR techniques mainly consist of producing either a local strain measurement or a distributed strain one, respectively. However, FBGs can be easily obtained in an array of many sensors and thus a quasi-distributed strain measurement can be obtained. On the other hand, the price to pay is more expensive sensors, complicated routes of the fibre (if FBGs are not contiguous as some production technologies require), uncertainty in the positioning of FBG on the specimen, and systematic errors due to a non-homogeneous strain (as is common in BF measurements). On the contrary, OBR has the advantage of a cheap standard fibre (allowing many strain profiles to be monitored) and a spatial strain resolution of about 1 mm; among its disadvantages, there are a lower sampling frequency, a higher interrogator cost, and the worse standard deviation of the measurements, in authors' experience about 20 μm/m for OBR with respect to 3 μm/m for FBG. Having applied both technologies, authors' preference is, at present, toward OBR, because of the possibility of measuring many strain profiles using only one optical fibre per specimen. Moreover, in an industrial perspective, the possibility of monitoring large parts with cheap fibres is an important advantage, as well.

The present work is an evolution, based on the OBR technology, of the BF monitoring technique using an array of FBG sensors presented in [5]. In order to demonstrate the possibility of exploiting the BF strain monitoring technique by OBR distributed sensing to monitor FCG in bonded joints, a validation by other techniques is required. In [5] some of the authors of the present paper compared the results of FCG monitoring based on strain measurements, performed using an array of FBG, to concurrent NDT of the same joint by Phased Array Ultrasonic Testing (PAUT) [18]. This is an advanced UT technique where an array of piezoelectric elements is electronically controlled in order to allow for operations (dynamic focusing, steering, *etc*.) not available using conventional UT probes. The most important feature of PAUT systems for the present research is the possibility of easily acquiring maps of what is inside the inspected body, like for medical echography.

The present paper presents the preliminary results of an experimental plan aiming at investigating the possibility of monitoring the structural health of adhesive joints by different methods. In this paper, the BF strain method, by OBR distributed sensing, is exploited to monitor FCG in a CFRP SL joint. The tested joint belongs to the same batch as the one tested in [17]. Fatigue cracks were also monitored by NDT techniques, *i.e.* VT and PAUT. The latter was used as a reference for validating the OBR results.

2. EXPERIMENTAL MONITORING OF FCG

The experimental monitoring of FCG was carried out considering one composite bonded SL joint subjected to fatigue cycles until failure.

2.1 Description of the Specimen

The specimen used for the FCG test is an SL adhesively bonded joint with CFRP adherends. Detailed dimensions of the specimen are shown in Fig. 1. The positions of the segments of the optical fibre used for the analysis described in the following sections are also reported schematically. Both adherends of the joint are woven CFRP laminate. The laminate is made of a stack of plain weave woven laminate consisting of low-modulus carbon fibres and epoxy matrix (more details on the material used can be found in [17]). The engineering constants of the woven CFRP are reported in Table 1. The

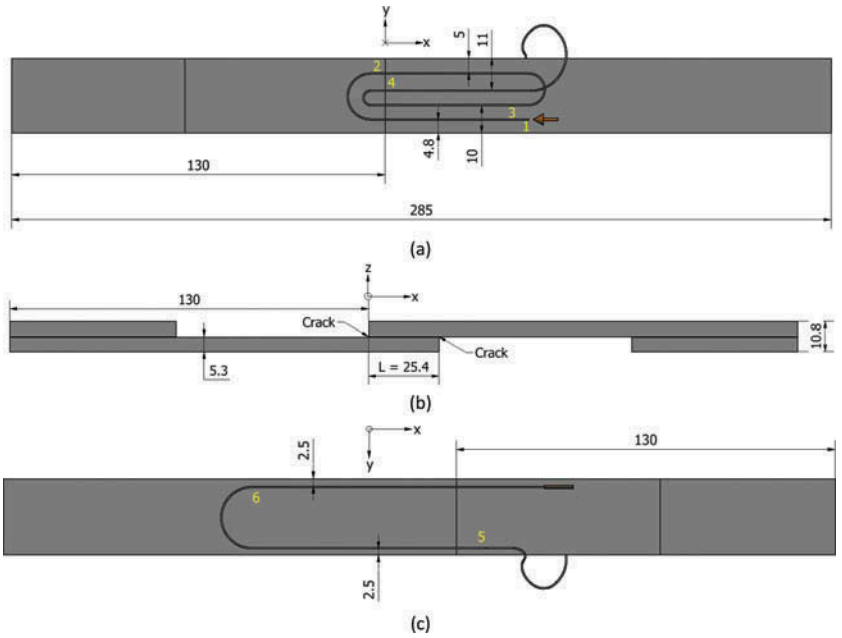

FIGURE 1 Drawing and dimensions of the tested specimen, with a schematic view of the position of the optical fibre segments used for strain measurement (dimensions in mm): a) top view; b) lateral view; c) bottom view.

TABLE 1 Engineering Constants of the Considered CFRP Composite

Young's moduli [MPa]	E_1 = 54,500	E_2 = 54,500	E_3 = 8000
Poisson's ratios	ν_{12} = 0.025	ν_{13} = 0.25	ν_{23} = 0.25
Shear moduli [MPa]	G_{12} = 5000	G_{13} = 2000	G_{23} = 2,000

stacking sequence is $[+45°/0°_2/+45]_s$ and the thickness of each lamina is 0.66 mm, which makes the total thickness of each adherend equal to 5.3 mm. The adherends were bonded by epoxy structural adhesive Scotch Weld 9323 B/A (3M Company, St. Paul, MN, USA) with an overlap of 25.4 mm. A uniform adhesive thickness was guaranteed by 0.2-mm-diameter glass spheres.

In order to understand the BF strain behaviour along the BF of the substrate, FE analyses were conducted using Abaqus v. 6.13 (Dassault Systèmes, Vélizy-Villacoublay, France). Several analyses were carried out for different crack lengths in order to realize the BF strain profile trend with respect to the crack. FE analyses were carried out using 3D solid, 20-node quadratic elements having an average edge length of 1 mm in the overlap region (considering mid-nodes, the node step was 0.5 mm). The full laminate was modelled with partitions having the properties of the corresponding plies. The adhesive layer was modelled using eight-node 3D cohesive elements with continuum response having an average edge length of 1.02 mm for the no-crack case (equally spaced nodes along 25.4 mm) and 0.2 mm thickness. The cohesive elements were connected to the upper and lower adherends using kinematic constraints (a possible alternative solution would consist of using 27-node solid elements for the adherends and let the nodes of the cohesive elements coincide with those on the surfaces of the adherends to connect, but this can make modelling of several crack lengths more complex).

In order to model the presence of cracks, two symmetric cracks stemming from the overlap ends (Fig. 1) were inserted by modifying the length and the position of the adhesive layer. Corresponding to the crack tips, transverse partitions were inserted in the models of the adherends, to let the crack front coincide with a line of nodes in the adherends, and kinematic constraints were modified accordingly.

All the displacements and rotations of the fixed end of the SL joint were constrained by suitable boundary conditions applied at nodes. On the load application end, only the displacement along the direction of the applied force was allowed. Nonlinearity due to geometry was taken into consideration. To quantify the differences between values along the centreline and in proximity to the edges, strain profiles were extracted for three given crack lengths (0, 6, and 11 mm) on the BF along two different longitudinal paths (identified by the labels “centreline” and “edge” in Fig. 2). Results are reported in Fig. 3. It appears that there is no significant difference between the strain profiles obtained across the width of the specimen for a 0 mm crack length, whereas differences become more evident for cracks longer than or equal to 6 mm.

The strain values, along the aforementioned paths, vary continuously and present a minimum peak value (Fig. 3), generated by the rotation of the joint during loading. It appears that, as the crack front is displaced in the model, the position of the minimum peak also moves in the same

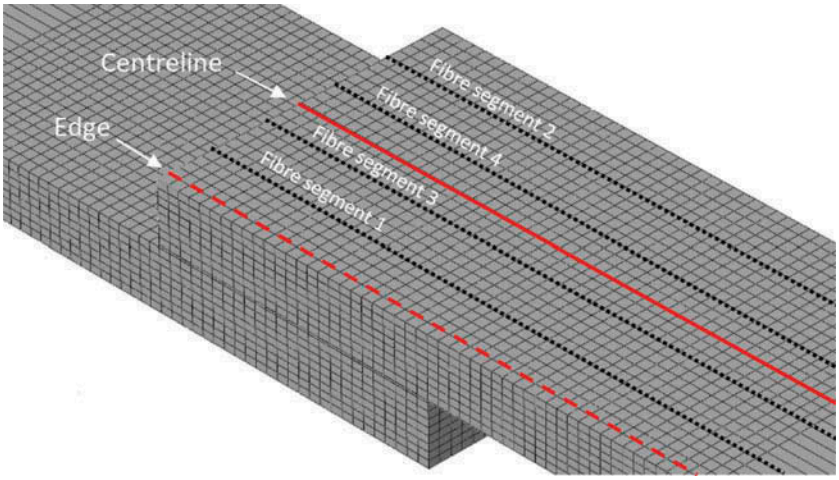

FIGURE 2 Finite Element model of the tested specimen.

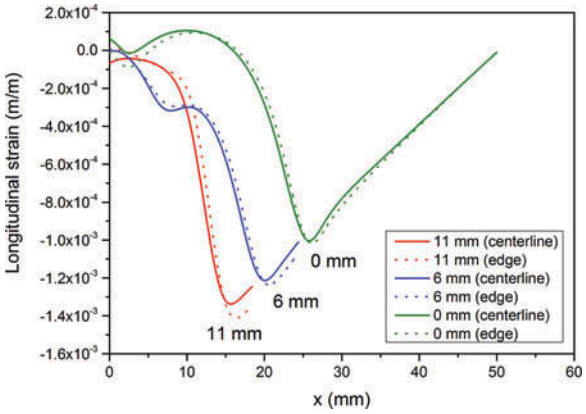

FIGURE 3 Strain profiles, extracted from the FE model, along the centreline and edge paths for three different crack lengths.

direction, thus suggesting a method to exploit this correlation and to infer the position of the crack by measuring the BF strain profile. In particular, the position x_{min} of the minimum longitudinal strain peak was identified by probing the nodal strain values and finding the minimum value. The distance between the identified node and the nearest overlap end (L-x_{min}, where L is the overlap length) was compared with the imposed crack length. Being the node step equal to 0.5 mm, this constitutes an upper bound estimate of the accuracy of the position of the minimum strain peak. The position (distance from the nearest overlap end) of the minimum strain peak is reported in Fig. 4 as a function of the crack length. Two sets of

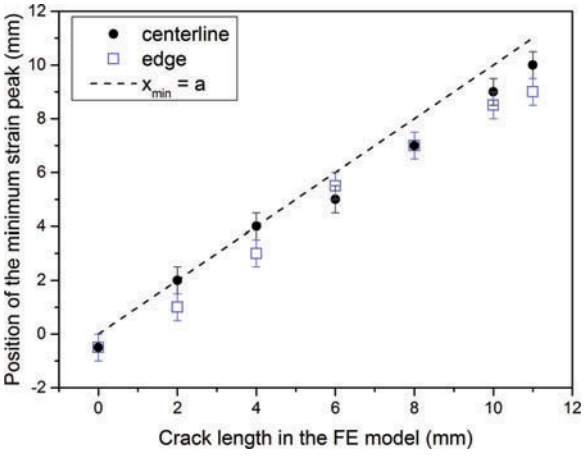

FIGURE 4 Position of the minimum peak of the numerical longitudinal strain as a function of crack length.

positions are considered, the ones extracted from longitudinal strain profiles along the centreline and the ones along the edges.

A reference dashed straight line having slope equal to 1, corresponding to a minimum peak position equal to the crack length a, is also plotted. It clearly appears that in a crack length range of 0–4 mm, the position of the minimum longitudinal strain recorded along the centreline almost coincides with the crack length. Deviations of the order of 1 mm appear for longer cracks. In the case of minima extracted along the edge path, deviations lie between 1 and 2 mm. In any case, it is possible to calibrate the relationship between the position of the minima and the crack length values, by finding the best fitting interpolation line. In both cases a linear relationship between the position of the minimum strain peak measured from the nearest overlap end (L-x_{min}) and the crack length a can be found, namely

$$L - x_{min} = 0.900\ a - 0.487 \tag{1}$$

for values extracted along the centreline and

$$L - x_{min} = 0.914\ a - 0.141 \tag{2}$$

for values extracted along the edge path.

Given the small differences observed in terms of position of the minimum peak of the longitudinal strain profiles through the width of the specimen, in this study all the experimental strain profiles were compared with the strain profiles extracted from the FE model along the centreline of the BF of one adherend.

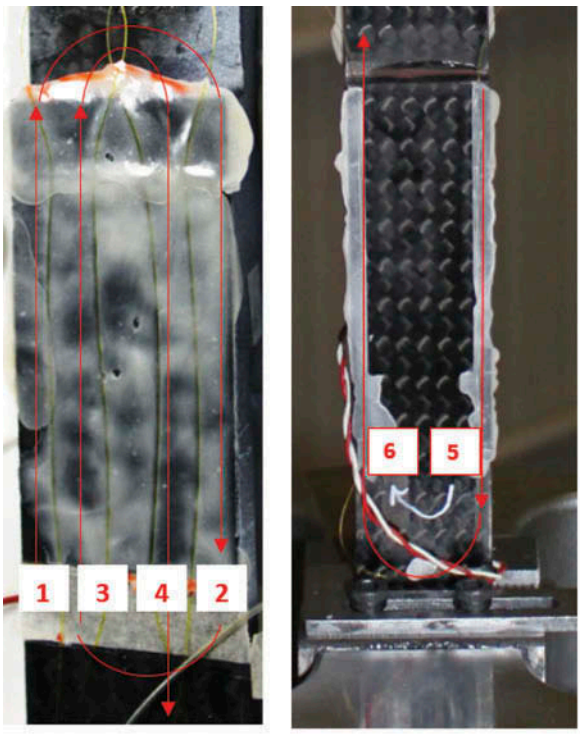

FIGURE 5 Application of fibre optic sensors to the specimen: a) four measuring fibre segments at the back surface; b) two measuring fibre segments at the front surface.

One single low bending optical fibre (type "Strain sensor 1 m", by Luna Innovations Inc., Roanoke, VA 24011, USA), equipped with an LC/APC connector and a low-reflection termination, was bonded on the top and bottom surface of the specimen in the overlap region, as shown schematically in Fig. 1 and as reported also in the picture of the actual specimen (Fig. 5). The fibre was bent in order to obtain four measuring segments that were bonded on one face, numbered 1, 3, 4 and 2, and two other segments, numbered 5 and 6, bonded on the other face. This other face was used also for UT; thus fibre segments were bonded very close to the edge of the specimen, in order to leave a smooth and free surface to be placed into contact with the PAUT probe, as shown in Fig. 6(a) and 6(b). Fibres were bonded using the two-components fast curing adhesive X60 (Hottinger Baldwin Messtechnik GmbH, Darmstadt, Germany); preparation of the surfaces followed a well-established chemical-mechanical procedure according to the strain gauges bonding procedure, where the surfaces were slightly abraded and then solvent cleaned. Fibres were kept in position and straight during curing using adhesive tape applied over the bent

segments outside the measuring area, while the adhesive was pressed using a thin polytetrafluoroethylene film.

2.2 Fatigue Crack Growth Experimental Set-up

The described specimen was fatigue tested in load control mode, using a uniaxial MTS 810 servo-hydraulic testing machine of 100 kN capacity. The cyclic load, chosen on the base of a previously obtained S-N curve of the joint, was characterized by an amplitude of 3.5 kN and a fatigue ratio R equal to 0.05. Under these conditions, the estimated 50% fatigue life was 50,000 cycles. A test frequency of 10 Hz was applied. The test was interrupted every 5,000 cycles so that VT by means of a digital camera, PAUT by a phased array unit, and strain measurements by an OBR interrogator could be performed with an applied static load corresponding to 3.8 kN, *i.e.* the mean value of the load cycle.

2.3 Crack Growth Monitoring Set-up

As a first monitoring approach, VT was carried out in order to evaluate the surface position and evolution of crack tips at the top and bottom ends of the SL joint. VT was performed on one side of the specimen after preliminary preparation using a white acrylic-based paint (Molotow 127H) to enhance crack contrast. The set-up consisted of a Canon EOS 500D camera equipped by an optical stabilized 18–55 mm lens and mounted on an adjustable tripod located at 500 mm distance from the specimen. Finally, a Bosch GLI DeciLed magnetic LED lamp was used to light up the target surface.

A Harfang X-32 Phased Array unit, equipped with a 5 MHz 32 active elements linear probe, allowed PAUT by means of longitudinal bulk waves. Figure 6 shows the inspection approach applied at the interruptions of the fatigue test (see Section 2.2). In detail, a "0° Linear-Scan" (L-Scan) phased array technique [18] was applied to inspect the front-side central region of the sample (Fig. 6(b)) due to the encumbrance of the optical fibres glued on the back one. As shown schematically in Fig. 6(c), a number of eight active elements were then sequentially activated, over the 32-element full array, allowing the collection of 50 ultrasonic beams and the inspection of the bonded region without moving the probe. Additionally, to improve lateral resolution, the half-step electronic scanning [18] was adopted. Finally, a dedicated ultrasonic gel guaranteed acoustic coupling between the probe and the specimen, while the calibration of the time axis showed that the speed of longitudinal waves in the sample was approximately equal to 2700 m/s.

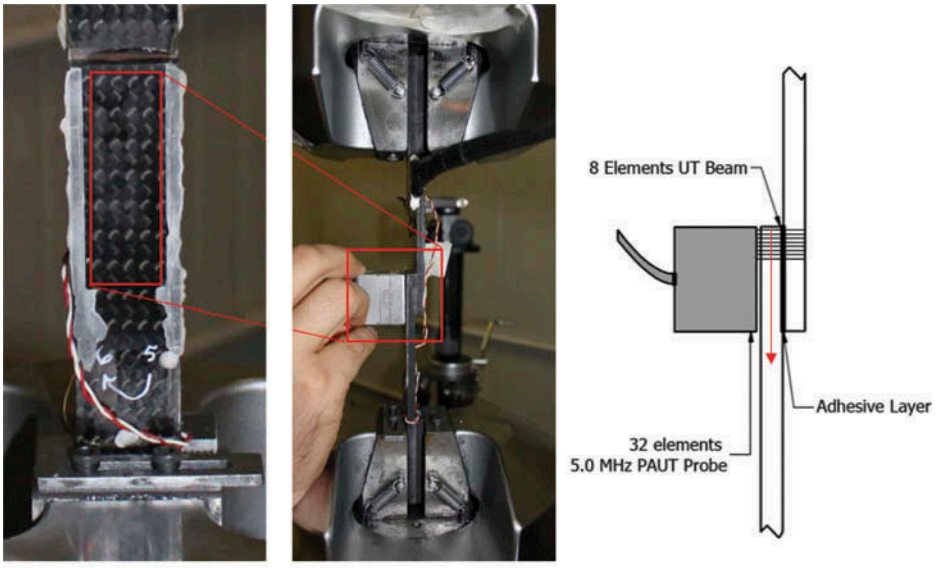

FIGURE 6 Phased array ultrasonic inspection set-up: a) and b) area inspected by manually coupled phased array probe; c) schematic representation of the working principle of electronic linear scanning.

An OBR interrogator, model ODiSI-B by Luna Innovations Inc., Roanoke, Virginia, USA, was used. OBR was used to measure the strain along the optical fibre. The measurement can be performed along the entire fibre with thousands of sensing locations interrogated simultaneously, transforming an ordinary optical fibre into a high spatial-resolution strain sensor. Strain values can be evaluated over discrete portions of the fibre, acting as virtual sensors defined as gauge length, which can be set by the operator in the OBR instrument. The adopted gauge length was 1.3 mm, with a gauge separation of 0.65 mm. Strain values were recorded at test interruptions as described in Section 2.2. The initial strain distribution was recorded, at 2 kN, for comparison purposes with the FE model and the trend along segments 1–4 is plotted in Fig. 7, superimposed on the strain values extracted along the centreline of the specimen from the FE model. It appears that the strain values agree well with the FE results, although they differ in terms of smoothness (OBR strain displays a waviness probably due to the non-uniform strain in the woven material, combined with the standard deviation of 20 μm/m of the used mode at 23.8 Hz with 1.3 mm spatial resolution) and values of the minimum peak (the FE model predicts a higher absolute value), whereas the average position of the minimum peak almost coincides with that obtained by FE analyses. It is also worth observing that, in this uncracked configuration, the minimum strain peak is located at the end of the overlapping region, *i.e.* at 25.4 mm.

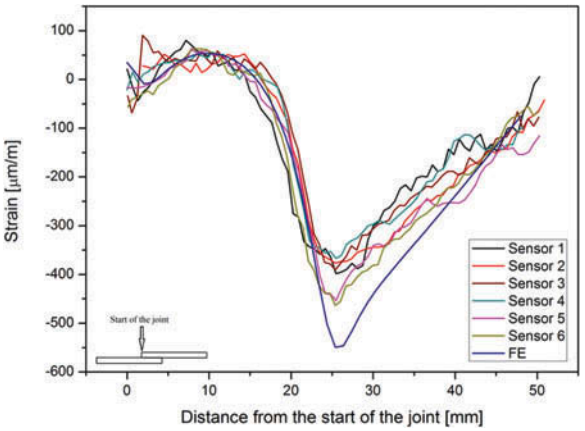

FIGURE 7 Finite Element estimation of longitudinal strain in the uncracked specimen compared to Optical Backscatter Reflectometry measurements.

3. RESULTS AND DISCUSSION

Eventually, the specimen lasted for 59,913 fatigue cycles before final failure with complete separation of the substrates. The results of VT, PAUT, and OBR strain measurements are reported in the following sections.

3.1 Visual Testing

Multiple acquisitions, one for each test interruption, were made available at the end of the test. As an example, Figure 8 shows two different cases at 30,000 and 59,846 fatigue cycles, respectively. All the acquired photographs

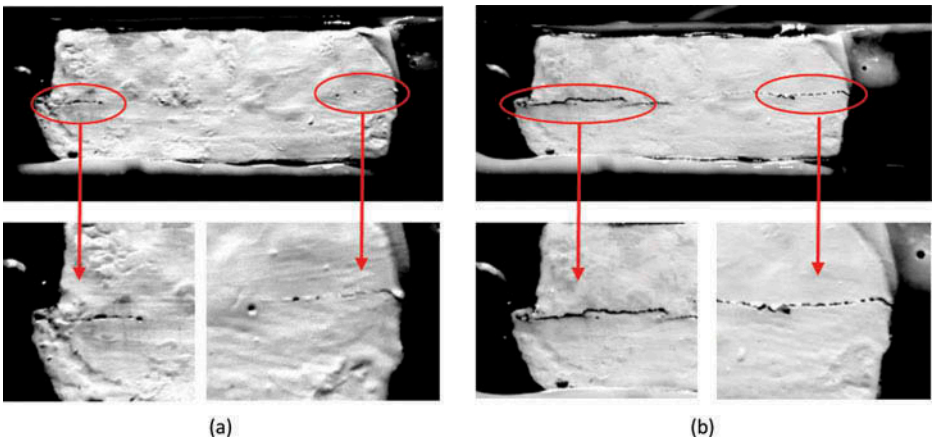

FIGURE 8 Visual inspection of the propagating crack: a) at 30,000 cycles; b) at 59,846 cycles.

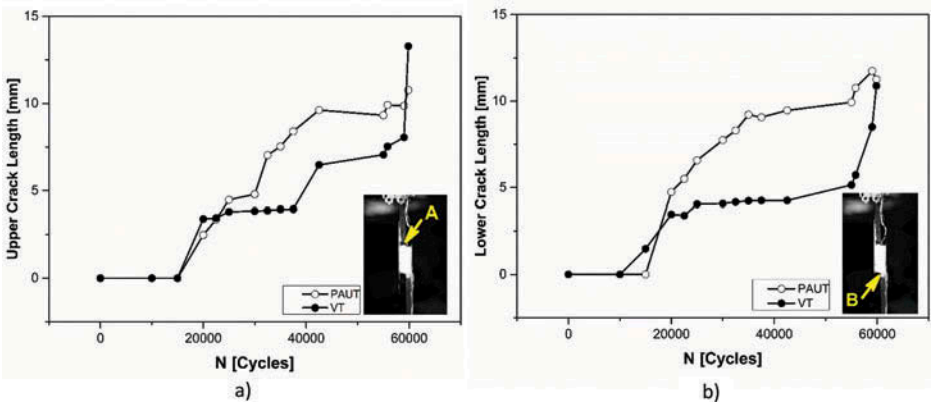

FIGURE 9 Visual testing and comparison to phased array ultrasonic testing: a) upper crack evolution; b) lower crack evolution.

were then digitally elaborated, after the suitable calibration of the pixel–length relationship, to size the evolution of the surface length of the cracks during the fatigue test. Figure 9 shows the obtained estimations, compared with the ones obtained by PAUT, as described in the following section.

3.2 Phased Array Ultrasonic Testing

The results obtained by an L-Scan represent the ultrasonic cross-section view of the specimen. In Fig. 10, two examples, from the fatigue test, are reported: the reference condition at 0 fatigue cycles and a damaged one after 30,000 fatigue cycles. Particularly, the former highlights three different characteristic

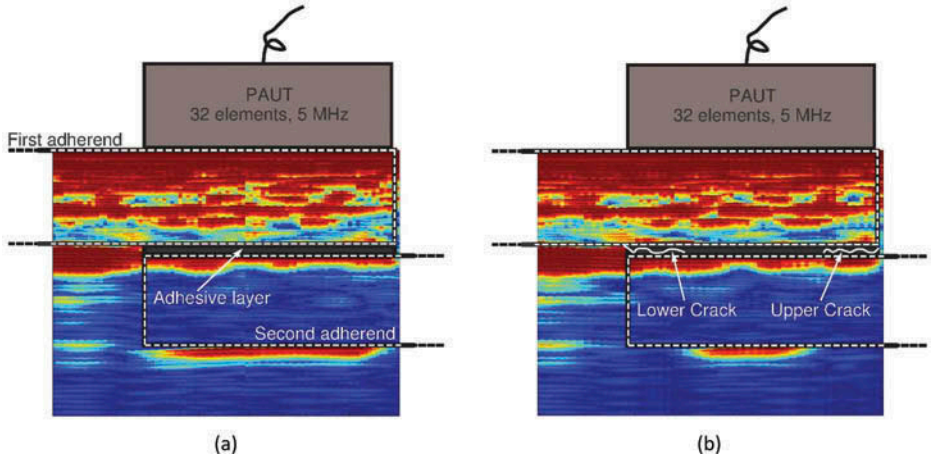

FIGURE 10 Phased array ultrasonic inspection: a) L-Scan at 0 fatigue cycles, b) L-Scan at 30,000 fatigue cycles.

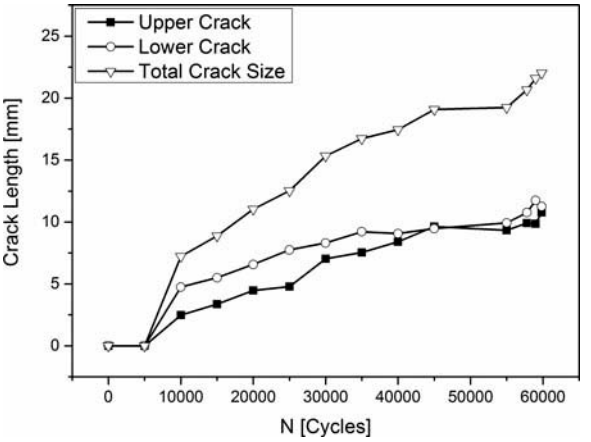

FIGURE 11 Crack sizing by phased array ultrasonic testing (-6 dB technique).

regions: i) at the left, the back-wall echo of a single CFRP adherend is evidenced; ii) in the centre, the bonded joint is characterized by the echo coming from the second CFRP adherend; and iii) at the right, the probe is coupled with air. As damage evolves within the bonded region, the UT echo coming from the second adherend is progressively reduced and its width allows crack sizing. In particular, Figure 10(b) shows the propagation of two different cracks starting from the two extremities of the bonded region. The length of the upper and lower cracks was estimated by means of the −6 dB amplitude drop technique [2] using, as a reference, the ultrasonic amplitude of the second adherend. The obtained estimations are reported in Fig. 11 as a function of fatigue cycles. Such estimations are characterized by an uncertainty of ±0.38 mm due to the spatial digitizing step of the electronic linear scanning. It is worth noting that the first stages of crack initiation and propagation could be barely monitored using the aforementioned PAUT technique, since its starting path was not perpendicular to the applied sound beam, but inclined at about 45°, thus reflecting the beam itself outside of the probe area. Consequently, no crack could be detected with respect to the baseline condition within the first 10,000 fatigue cycles.

3.3 Comparison Between Phased Array Ultrasonic Testing and Visual Testing

Figure 9 shows, qualitatively, similar trends between VT and PAUT results, but significantly different estimated crack length values, as well. It is worth remarking that PAUT measurements were carried out in the centre of the joint (see Fig. 6), while VT was performed on the external side of the sample. Thus, beyond the relevant and characteristic uncertainties of the two methods, it is reasonable to assume a curved crack front due to different plane stress

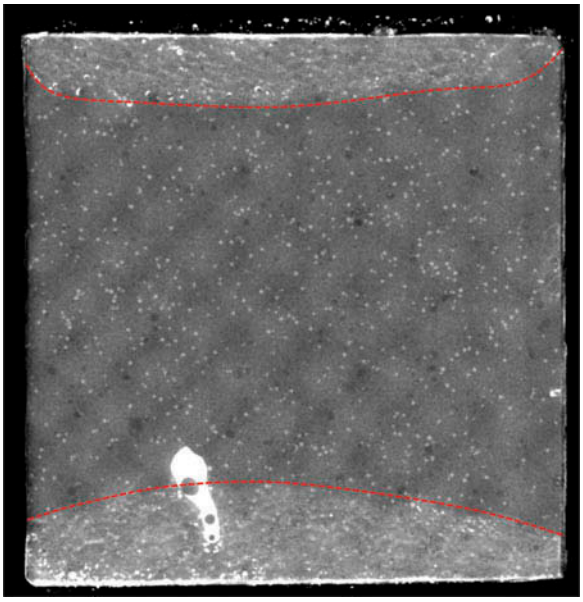

FIGURE 12 X-ray digital radiography of a fatigue-tested specimen nominally equivalent to the monitored and inspected one.

and plane strain conditions along the specimen width. In particular, the central region of the specimen is likely to be subjected to anticlastic bending moments leading to a plane strain state, which leads to a higher crack growth rate, while, at the specimen's edges, a generalized plane stress condition should prevail and rule the phenomenon. To support this hypothesis, a 2D digital radiography (DR) X-ray inspection of another specimen, geometrically identical and fatigue tested with the same load conditions as the monitored one, was performed using a North Star Imaging 3D X-Ray CT X25 system. The adopted X-ray source parameters were 76 kV and 40 μA, while a focal spot size of 3 μm and a frame averaging of 3.3 ms were employed. Moreover, throughout the fatigue test, the specimen was subjected to infiltration by a specially prepared liquid to enhance the DR image contrast. The radiography reported in Fig. 12 clearly reveals a curved cracked front, consistent with the VT observation of shorter cracks at specimen edges and of longer ones, along the specimen centreline, by PAUT inspection.

3.4 Strain Profiles Recorded by Optical Backscatter Reflectometry

During the fatigue test, strains were recorded at mean load every 5,000 cycles. Values of the strain recorded along segment 4 are reported in Fig. 13. The strain pattern evolved as expected, with the shape found by FE analysis and a translation of the negative peak with the number of cycles up to 30,000 cycles,

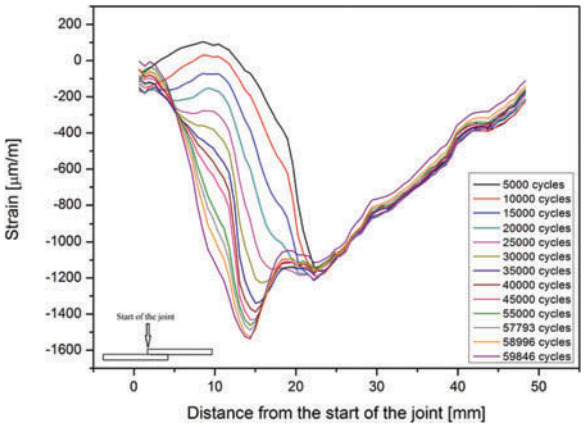

FIGURE 13 Longitudinal strain profiles measured by Optical Backscatter Reflectometry at different number of cycles (example from OBR segment 4).

following the displacement of the crack front. Afterwards, the shape of the strain profile changed, although maintaining the characteristic feature of a sharp negative peak, travelling towards the centre of the overlap, again because of the translation of the crack front. A similar behaviour was observed in the strain profiles extracted along the other segments, although differences were apparent, as shown in Fig. 14, where the strain profiles recorded at 30,000 cycles along segments 1–4 are plotted.

At this stage of the fatigue test, PAUT inspection revealed a 7-mm-long lower crack on the corresponding side of the overlap. Accordingly, in Fig. 14, the strain profile extracted along the centreline of the FE model for a 7-mm crack length is superimposed to experimental values. A good agreement is

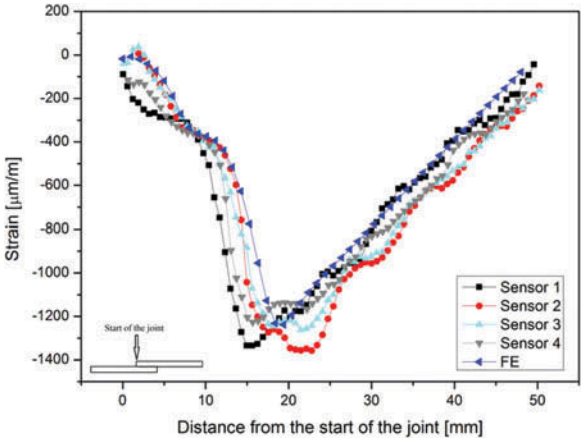

FIGURE 14 Comparison of Optical Backscatter Reflectometry results to finite element analysis considering a 7-mm-long one-sided crack.

found, in terms of both shape of the strain profile and average position of the minimum peak. However, it is important to highlight that the four segments provided four different values of the position of the negative peak. This suggested evaluating an average position of the negative peak, for comparison with VT and PAUT observations, as discussed in the following section.

3.5 Comparison Between Phased Array Ultrasonic Testing and OBR

Averaged values of the position of the negative peak of the strain profile recorded by the OBR interrogator along the segments are plotted as a function of the number of cycles in Fig. 15. Segments 1–4 provided values

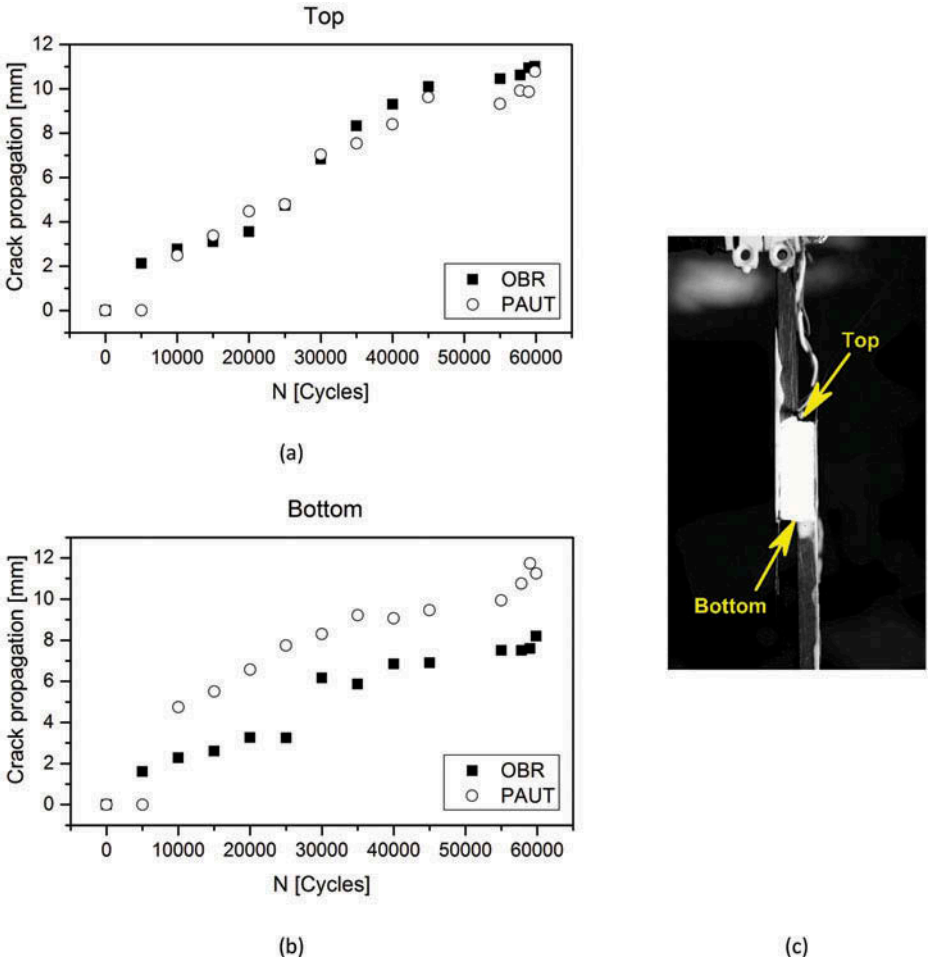

FIGURE 15 Comparison between the positions of the crack, inferred through the position of the minimum strain peak recorded by Optical Backscatter Reflectometry, and of the crack front detected by phased array ultrasonic testing.

referring to the propagation from the top edge of the overlap, whereas segments 5 and 6 are from the bottom edge. The position of crack fronts measured by PAUT is superimposed. Figure 15(a) shows a good agreement between OBR and PAUT measurements from the top edge. Conversely, the results reported in Fig. 15(b), which refers to a crack propagating from the bottom edge, display an offset, between OBR and PAUT, which varies between 2 and 4 mm, depending on the number of cycles. This can be explained observing again Fig. 12 and remembering that measurements for monitoring crack propagation from the bottom edge of the specimen adopted just two OBR located very close to its edges (shorter crack) and PAUT inspection at its centreline (longer crack). However, a similar trend is observed.

These preliminary results seem to confirm that, by measuring the strain profile in the overlap region accurately, a correlation between the minimum peak of the strain profile and the position of the crack tip exists. This correlation, if confirmed by further testing, could be exploited for monitoring the structural health of these kinds of joints. However, testing of more specimens and comparison of results with those obtained by other inspection techniques like ultrasonic Lamb waves (the wiring of these sensors is visible in Figs. 5 and 6) are required and tests are already being conducted by the authors of the present paper.

4. CONCLUSIONS

In this paper, the results of monitoring fatigue crack propagation in an adhesively bonded composite joint by different techniques are presented. First, by measuring the strain profile on the BF of the joint using OBR distributed sensing technique, the full strain profile is recorded. The profile presents a minimum strain peak and the proposed monitoring technique is based on the identification of the position of this negative peak. Then the crack was monitored by VT of the side of the joint using a camera. Finally, using phased array ultrasonic technique, the position of the cracks stemming from both ends of the overlap was measured.

Based on the results presented in this paper, the following conclusions can be drawn:

- the OBR technology allows for measuring accurately the BF strain profile in SL joints and the intrinsic distributed sensing capabilities allowed for measuring the position of the minimum strain peak typical of SL joints;
- FE analyses indicated that, as a crack forms at one or both ends of the joint in the adhesive layer, the minimum strain peak is displaced linearly with crack length;

- during a fatigue test, by comparing the position of the minimum strain peak with the position of the crack front measured by PAUT, a good agreement was found;
- the obtained results have to be considered as preliminary, particularly because they are based on one single test; however, they are encouraging and seem to indicate that, thanks to its distributed sensing capabilities, the OBR technology could allow for exploiting better the BF technique, as well as any other strain field-based technique, for the health monitoring of adhesive bonded SL joints.

ACKNOWLEDGEMENTS

The authors would like to acknowledge the use of experimental facilities available at Politecnico di Milano within the frame of the following interdisciplinary laboratories: "AMALA" for digital radiography, "LAFOS" for OBR, and "PoliNDT" for PAUT measurements.

REFERENCES

[1] Adams, R. D. and Drinkwater, B. W., *NDT&E Int*. **30**, 93–98 (1997).
[2] Kraütkramer, J., Kraütkramer, H., *Ultrasonic Testing of Materials*, (Springer-Verlag, Berlin, Germany, 1990) 4th Edition.
[3] Zhang, Z. and Shang, J. K., J. *Adhes*. **49**, 23–36 (1995).
[4] Crocombe, A. D., Ong, C. Y., Chan, C. M., Abdel Wahab, M. M., Ashcroft, I. A., J. *Adhes*. **78**, 745–778 (2002).
[5] Bernasconi, A., Carboni, M., Comolli, L., *Procedia Eng*. **10**, 207–212 (2011).
[6] Bernasconi, A., Comolli, L., Proc. *SPIE*. **8421**, 84214Y (2012).
[7] Canal, L. P., Sarfaraz, R., Violakis, G., Botsis, J., Michaud, V., Limberger, H. G. Compos. *Struct*., **112**, 241–247 (2014).
[8] Sans, D., Stutz, S., Renart, J., Mayugo, J. A., Botsis, J. *Compos. Struct*. **94**(9), 2879–2887 (2012).
[9] Stutz, S., Cugnoni, J., Botsis, J., Compos. *Sci. Technol*. **71**(4), 443–449 (2011).
[10] da Silva, L. F. M., Moreira, P. M. G. P., Loureiro, A. L. D. J. Adhes. *Sci. Tech*. **28** (14–15), 1480–1499 (2014).
[11] Sanderson, A. R., Ogin, S. L., Crocombe, A. D., Gower, M. R. L., Lee, R., *J. Compos. Sci. Technol*. **72**(10), 1121–1126 (2012).
[12] Capell, T. F., Palaniappan, J., Ogin, S. L., Crocombe, A. D., Reed, G. T., Thorne, A. M., Mohanty, L., Tjin, S. C., *J. Opt. A. – Pure Appl. Opt*. **9–6**, 40–44 (2007).
[13] Palaniappan, J., Wang, H., Ogin, S. L., Thorne, A. M., Reed, G. T., Crocombe, A. D., Mohanty, L., Rech, Y., Tjin, S. C., Comp. *Sci. Tech*., **67**, 2487–2853, (2007).
[14] Güemes, A., Fernandez-Lopez, A., Soller, B., Struct. *Health Monitor*. **9**(3), 233–245 (2010).

[15] Frövel, M., Del Olmo, E., Fernández, A., Quero, F., Carrión, G., Pintado, J. M., Güemes, A. *6th European Workshop on Structural Health Monitoring* (2012). *Damage detection by load path changes in reinforced composite panels using local FBGs and distributed sensing*.
[16] Grave, J. H. L., Håheim, M. L., Echtermeyer, A. T. *Evaluation of the Strain Field in a Composite-Metal Adhesive Joint with an Optical Backscatter Reflectometer*, ECCM 15, Venice, Italy.
[17] B: Bernasconi, A., Kharshiduzzaman, M., Comolli, L., *J. Adhes*. (2015) DOI:10.1080/00218464.2015.1043005.
[18] Schmerr, L. W., *Fundamentals of Ultrasonic Phased Arrays*, Berlin, Germany, Springer-Verlag, 2015.